NAVAL MEDICAL RESEARCH INSTITUTE

Bethesda, MD 20889-5055

NMRI 91-39 July 1991

BASIC OPERATION AND PRELIMINARY TRIALS OF A DETECTOR FOR STATIONARY GAS BUBBLES

G. Albin
P. Massell
E. Thalmann

Naval Medical Research
and Development Command
Bethesda, Maryland 20889-5044

Department of the Navy
Naval Medical Command
Washington, DC 20372-5210

NOTICES

The opinions and assertions contained herein are the private ones of the writer and are not to be construed as official or reflecting the views of the naval service at large.

When U. S. Government drawings, specifications, or other data are used for any purpose other than a definitely related Government procurement operation, the Government thereby incurs no responsibility nor any obligation whatsoever, and the fact that the Government may have formulated, furnished or in any way supplied the said drawings, specifications, or other data is not to be regarded by implication or otherwise, as in any manner licensing the holder or any other person or corporation, or conveying any rights or permission to manufacture, use, or sell any patented invention that may in any way be related thereto.

Please do not request copies of this report from the Naval Medical Research Institute. Additional copies may be purchased from:

National Technical Information Service
5285 Port Royal Road
Springfield, Virginia 22161

Federal Government agencies and their contractors registered with the Defense Technical Information Center should direct requests for copies of this report to:

Defense Technical Information Center
Cameron Station
Alexandria, Virginia 22304-6145

TECHNICAL REVIEW AND APPROVAL

NMRI 91-39

The experiments reported herein were conducted according to the principles set forth in the current edition of the "Guide for the Care and Use of Laboratory Animals," Institute of Laboratory Animal Resources, National Research Council.

This technical report has been reviewed by the NMRI scientific and public affairs staff and is approved for publication. It is releasable to the National Technical Information Service where it will be available to the general public, including foreign nations.

LARRY W. LAUGHLIN
CAPT, MC, USN
Commanding Officer

REPORT DOCUMENTATION PAGE

1a. REPORT SECURITY CLASSIFICATION UNCL	1b. RESTRICTIVE MARKINGS
2a. SECURITY CLASSIFICATION AUTHORITY	3. DISTRIBUTION/AVAILABILITY OF REPORT Approved for public release; distribution is unlimited
2b. DECLASSIFICATION/DOWNGRADING SCHEDULE	
4. PERFORMING ORGANIZATION REPORT NUMBER(S) NMRI 91-39	5. MONITORING ORGANIZATION REPORT NUMBER(S)
6a. NAME OF PERFORMING ORGANIZATION Naval Medical Research Institute 6b. OFFICE SYMBOL (If applicable)	7a. NAME OF MONITORING ORGANIZATION Naval Medical Command
6c. ADDRESS (City, State, and ZIP Code) 8901 Wisconsin Avenue Bethesda, MD 20814-5055	7b. ADDRESS (City, State, and ZIP Code) Department of the Navy Washington, DC 20372-5120
8a. NAME OF FUNDING/SPONSORING ORGANIZATION Naval Medical Research & Development Command 8b. OFFICE SYMBOL (If applicable)	9. PROCUREMENT INSTRUMENT IDENTIFICATION NUMBER
8c. ADDRESS (City, State, and ZIP Code) 8901 Wisconsin Avenue Bethesda, MD 20814-5044	10. SOURCE OF FUNDING NUMBERS PROGRAM ELEMENT NO. 63713N; PROJECT NO. M0099; TASK NO. 1002; WORK UNIT ACCESSION NO. DN177792

11. TITLE (Include Security Classification)

(U) BASIC OPERATION AND PRELIMINARY TRIALS OF A DETECTOR FOR STATIONARY GAS BUBBLES

12. PERSONAL AUTHOR(S)
Gary Albin, Paul Massell, Edward Thalmann

13a. TYPE OF REPORT	13b. TIME COVERED	14. DATE OF REPORT (Year, Month, Day)	15. PAGE COUNT
Technical Report	FROM 09/88 TO 05/89	1991 July	47

16. SUPPLEMENTARY NOTATION

17. COSATI CODES			18. SUBJECT TERMS (Continue on reverse if necessary and identify by block number)
FIELD	GROUP	SUB-GROUP	Bubbles, bubble detection, ultrasonic, harmonic, resonance, decompression sickness, doppler

19. ABSTRACT (Continue on reverse if necessary and identify by block number)

A unique system has been developed to detect stationary gas bubbles 1 to 20 μm in diameter by using ultrasonic interrogation. We describe the system and propose a protocol for using it to identify the sizes and numbers of bubbles. A mathematical model of a vibrating bubble in liquid has been coded into a computer program, and currently we are developing an analogous model to simulate a bubble in an elastic solid. A technique is described for preparing calibration standards by trapping bubbles in a transparent hydrogel, which can be assayed using light microscopy. Crude preliminary trials with the bubble detector demonstrate that it can detect sufficiently large populations of bubbles, although its signal/noise ratio appears too low for detecting individual bubbles. Quantitative assay of bubbles is not possible until the system has been modified to provide a way to capture and store the output signal.

20. DISTRIBUTION/AVAILABILITY OF ABSTRACT	21. ABSTRACT SECURITY CLASSIFICATION	
☒ UNCLASSIFIED/UNLIMITED ☐ SAME AS RPT ☐ DTIC USERS	Unclassified	
22a. NAME OF RESPONSIBLE INDIVIDUAL Regina E. Hunt, Command Editor	22b. TELEPHONE (Include Area Code) (202) 295-0198	22c. OFFICE SYMBOL SD/RSD/NMRI

TABLE OF CONTENTS

ACKNOWLEDGEMENTS

We are greatly indebted to Mr. William Mints (NMRI) for tutoring us in electrical engineering principles. Our thanks to Dr. Nick Peppas (Purdue University) for advice on the mechanical properties of hydrogels. Finally, we thank Ms. Joanne Lum for the experimental work discussed in this report.

This work was supported by the Naval Medical Research and Development Command Work Unit No. 63713N M0099.01A-1002. The opinions or assertions contained herein are the private ones of the authors and are not to be construed as official or reflecting the views of the Navy Department or the naval service at large.

INTRODUCTION

Symptoms of decompression sickness (DCS) typically are assumed to result from the formation of gas bubbles in blood or extravascular tissue. Information on extravascular bubbles has been severely limited by the lack of any non-destructive method of observing them.

The Jet Propulsion Laboratory (JPL) (Pasadena, California) has constructed and delivered a system that uses ultrasound to detect stationary gas bubbles. This was done under a work order from the Naval Medical Research and Development Command (NMRDC) following JPL Proposal No. 70-2204. We call the system the "JPL swept-frequency bubble detector" but in this report we usually will refer to it as simply the "bubble detector." The bubble detector can, in principle, enable one to quantitatively measure the sizes and numbers of stationary extravascular bubbles. Its theory of operation depends on the facts that 1) gas bubbles are the softest objects in tissue, and consequently vibrate at the highest amplitudes when excited by sound, 2) although vibrations are linear at sufficiently low amplitudes, they become increasingly nonlinear with increasing amplitude (1), and 3) nonlinear oscillations contain harmonics and subharmonics -- that is, the vibrations contain multiple frequency components even when the driving signal is monotonal. Therefore it is expected that, when tissue is driven to vibration by externally applied sound that is not too high in amplitude, any harmonics or subharmonics in the sound backscattered from the tissue should be attributed only to gas bubbles rather than stiffer objects. More specifically, the bubble detector allows one to use the "second harmonic" component of the energy backscattered by vibrating bubbles (the component with a frequency twice that of the driving signal) to characterize a bubble population. Equations derived by Prosperetti predict the amplitude vs. driving frequency relationship (i.e., the amplitude spectrum) for this second harmonic component as a function of bubble size for a single, free, spherical bubble in an infinite liquid (2,3). However, there is a lack of direct experimental verification of these equations. There does appear to be empirical confirmation of the most interesting prediction of

Prosperetti's equations, which is the appearance of maxima in the amplitude spectrum at certain "resonance frequencies." At least three groups have reported observing increased amplitude of the second harmonic component near the so-called "main resonance" frequency (4-6).

The bubble detector uses a transmit pressure transducer to broadcast a swept-frequency sound pressure field onto a target, and a receive pressure transducer to detect the backscattered sound waves from the target. It then filters out and discards all frequency components in the output signal except for either the second harmonic or the "fundamental" (the component having the same frequency as the driving signal), as desired. The two filtered components are then processed to give two types of conditioned output signals. In the "range" mode the system produces an amplitude spectrum in which the x variable consists of the difference in frequency between the transmitted and received signals. This frequency offset is proportional to the time delay between sound transmission and reception of the backscattered sound from the target, so the distance from the transducer head to the target is easily calculated from it. Each target has a unique frequency offset that depends on its distance from the transducers' head.

In the "frequency response" or "FRC" mode the system generates a spectrum in which the x variable is the driving frequency and the y variable is a function of the amplitude of the backscattered signal from any targets that are a certain (selectable) distance from the transducers. This output is equivalent to the "frequency response" of the system comprising both the bubble and the bubble detector -- that is, it shows how strongly the system responds to its input as a function of the input frequency. In theory, it provides the information enabling one to assay a bubble population: the location of a resonance peak in the spectrum depends on the bubble diameter and the peak size is proportional to the number of bubbles at that diameter. The transducers supplied by JPL are designed to operate in a frequency range that encompasses the main resonance frequencies of bubbles of roughly

1-20 microns in diameter, so we can theoretically expect to be able to identify bubbles in this size range.

For a sample containing an unknown bubble population, we expect to deduce the sizes and numbers of bubbles using a standard curve-fitting/parameter estimation approach: we will fit a curve to the spectrum obtained in the FRC mode, with the values of bubble diameter and bubble number taken as adjustable parameters to be optimized in the curve-fitting routine. It is understood that the optimized values of bubble diameter and bubble number will not accurately represent the bubble population unless accurate values of the important physical parameters (viscosity, surface tension, etc.) are used in the fitted equation. This point implies that there will be considerable uncertainty in the results obtained when interrogating a system as difficult to characterize as tissue, and *in vivo* data may never be more than semi-quantitative. Nevertheless, it remains an advantage of this approach to data analysis that the optimized parameter values represent objective data rather than subjective interpretations of what may often be a complicated amplitude spectrum.

The first major goal is to identify or develop equations that describe vibrating bubbles in both liquids and elastic solids; this will be discussed in the section on "Gas Bubble Oscillations." These equations must then be incorporated into a computer program that predicts the output voltage amplitude of the bubble detector as a function of the relevant parameters and fits the prediction to the measured output voltage using SSE minimization, as will be discussed in "Data Handling." Next, we must calibrate the system by measuring the frequency responses of known bubble populations. A protocol has been developed for preparing these by trapping gas bubbles in transparent hydrogels and determining the sizes and numbers of bubbles in the gels microscopically; this procedure is outlined in "Preparation and Examination of Hydrogel Samples." Preliminary semi-quantitative experiments with bubbles in hydrogels, which are presented in the "Preliminary Trials with the JPL Bubble Detector," indicate that the signal/noise ratio of the system as delivered is

quite low. We discuss steps that are being taken to improve the system's performance in "Conclusions and Recommendations."

GAS BUBBLE OSCILLATIONS

This section will be a brief summary of only those aspects of gas bubble physics that are important to developing equations applicable to the JPL swept frequency bubble detector.

If a gas bubble is subjected to a periodic pressure oscillation superimposed upon the ambient pressure (i.e., a sound field), the resultant oscillation of its internal pressure causes it to vibrate in sympathy with the driving sound, generating spherical sound waves as it does so. When conditions are such that the various transport processes that occur in the bubble and the surrounding medium become out-of-phase with the oscillations of its radius, then the vibrations become "nonlinear." In a nonlinear system the magnitude of the output signal is not proportional to the magnitude of the input signal. In the case of the forced oscillation of a gas bubble, this means that the amplitude of changes in the radius is disproportionate to the amplitude of the externally imposed sound. A spectral analysis of the sound transmitted from the bubble surface would then reveal a component of the same frequency as the driving signal (i.e., the fundamental component) plus a number of "subharmonic" components (at frequencies f/2, f/3, etc., where f is the driving frequency) and "harmonic" components (at frequencies 2f, 3f etc.). Frequency 2f is the second harmonic frequency. The amplitudes of these frequency components are predicted to maximize when the driving signal is near certain resonance frequencies. The largest maximum occurs when f is near the natural frequency, which will be designated f_0, and is called the main resonance. Smaller maxima occur near $f=f_0/2$, $f=2f_0$, $f=f_0/3$, $f=3f_0$, etc.

For analyzing data from the bubble detector, an equation is needed to predict the amplitude of the second harmonic component of the radial oscillations of a gas bubble as a function of the frequency and amplitude of the externally imposed sound. This equation should be an analytic expression amenable to data-fitting using an iterative routine that minimizes the sum of squares of error (SSE); one or more differential equations requiring numerical solution would likely require excessive computer time. An equation that

incorporates no questionable assumptions and has been empirically verified does not appear to have been developed. However, Prosperetti has published several papers (2,3,7-9) treating the forced oscillation of a single, free, spherical bubble in an infinite, homogeneous, isotropic Newtonian liquid which have received at least partial experimental support. He has published only stationary-state solutions and assumes that the wavelength of the externally applied pressure oscillations is large compared with the bubble diameter, so that the bubble may be considered subjected to uniform external pressure. Interaction between two or more vibrating bubbles has not been treated yet in conjunction with nonlinear theory.

In a 1977 paper (3) Prosperetti solved the mass, energy, and momentum balances for a vibrating bubble and the surrounding liquid, using a first-order linearization to approximate the time derivatives of pressure, temperature, density, and bubble radius. The viscosity and mass of the gas phase were neglected. He did account for the compressibility of the liquid, i.e., the finite velocity of sound. The resulting analytic solution allowed him to quantify the major damping factors: viscous, thermal (caused by the out-of-phase oscillations of pressure and temperature within the bubble), and acoustic (caused by momentum transfer to the liquid from the bubble surface). The solution is strictly valid only for linear, monotonal oscillations. In particular, in the momentum balance on the liquid he used an expression for pressure at the inner bubble surface that depends on the temperature and pressure being exactly 180° out of phase, despite the phase shift imposed by a finite heat transfer rate. The thermal and acoustic damping factors were written in terms of effective thermal and acoustic viscosities, which could be summed with the liquid viscosity for substitution into the momentum balance.

In an earlier, 1974 paper (2), Prosperetti considered the nonlinear vibrations of a bubble in an incompressible liquid. Such an approach is valid near the bubble surface, where the time scale of sound wave propagation is small compared with the period of oscillation (10). Thermal damping was ignored and acoustic damping vanishes for an incompressible fluid. Under the

above assumptions he solved the momentum balance on the liquid using the Krylov-Bogolyubov-Mitropolsky asymptotic method (11) after approximating the derivatives with third-order expansions. Prosperetti used the same expression for pressure at the bubble inner surface, valid only for linear oscillations, as he published in the later, 1977 paper. The expression contains an "effective polytropic exponent" which governs the temperature within the bubble, and he used values of this parameter predicted by the linear theory, even though he was calculating nonlinear behavior. In spite of these simplifying assumptions, his results agree well with an earlier numerical solution to the momentum balance (12) and with experimental results (13). The experiments consisted of measuring the sound pressure level at a given frequency necessary to hold a bubble stationary in water by countering its buoyancy, which is a function of the amplitude spectrum of the radial oscillations. The agreement between theory and data is remarkably good in view of their highly irregular behavior when the driving frequency was near the bubble's main resonance frequency. This sort of experiment is not, however, a direct test of the theory's predictions regarding the second harmonic component of the radial oscillations.

We intend to use the analytic expressions from Prosperetti's 1974 paper, modified by the additions of thermal and acoustic damping as predicted by the linear theory presented in his 1977 paper. Appendix A summarizes this approach; equation [A3] is the function ultimately used to generate predictions of the pressure radiated from bubbles. Figure 1, which was generated using equation [A3], illustrates the behavior predicted by this approach for a 20-μm-diameter bubble in H_2O driven by externally applied pressure of amplitude $3 \cdot 10^5$ dyn/cm^2 (0.3 atm). The amplitude of the second harmonic component of the pressure (dimensions dyn/cm$^2 \cdot 10^{10}$) radiated back from the bubble at a distance of 3.25 cm is plotted in Figure 1 against a dimensionless driving frequency. The dimensional driving frequency varies between 0.12 MHz and 0.56 MHz for the data plotted in Figure 1. In Prosperetti's development the "natural frequency" f_0 of the bubble is actually

Figure 1: Predicted amplitude spectrum, 2nd harmonic of the pressure radiated from a 20 um-diameter bubble in H20

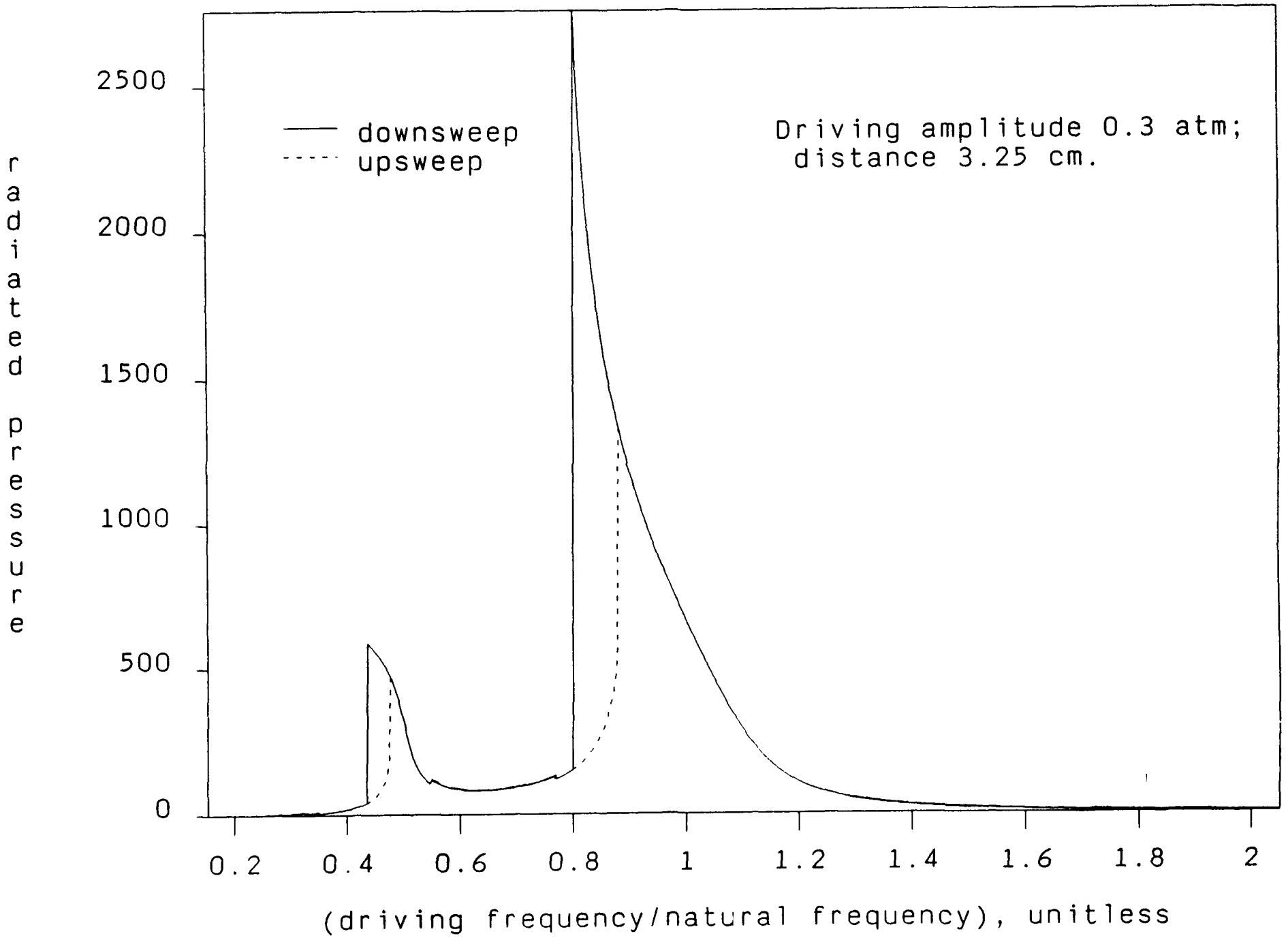

a function of driving frequency. For this bubble f_0 is very close to 0.35 MHz for all driving frequencies between 0.12 MHz and 0.56 MHz. The larger peak in Figure 1 is the main resonance peak, the smaller one is at the first harmonic frequency. Prosperetti's equations describe a so-called catastrophic system, named for the discontinuous "jumps" between stable states. The vertical left side of the main resonance peak is an example of this. Hysteresis is another characteristic of catastrophic systems; the dotted curve in Figure 1 corresponds to a sweep up in driving frequency (from 0.12 to 0.56 MHz) and the solid curve is for a sweep down (0.56 MHz to 0.12 MHz).

Recall that the equation used to generate Figure 1 is written for a single bubble. In a dense population of vibrating bubbles there actually is interaction between bubbles, i.e., the bubbles excite one another. The amount of interaction depends on the proximity of the bubbles to one another since the amplitude of a spherical sound wave is inversely proportional to the distance from its apparent point source, which in this case is the center of the vibrating bubble generating the wave. There does not appear to be a published theoretical development that treats the behavior of either 1) individual bubbles in a population of vibrating bubbles or 2) nonlinearly oscillating bubbles in a population. We therefore have chosen to use the single-bubble equations described in Appendix A.

DATA HANDLING

In its "frequency response" mode the bubble detector provides an output voltage amplitude, which is a function of driving frequency. It is necessary to relate that information to the input voltage and the relevant physical parameters in such a way that the bubble radius R_0 and the number of bubbles n_{bub} can be estimated. Equation [A3] from Appendix A, which arises from physics arguments, is used in making this connection between the raw data and the bubble size. Briefly, we will deduce R_0 and n_{bub} by fitting the data with a mathematical model of the physical system using a standard data-fitting/parameter estimation scheme, the Marquardt least-squares algorithm (14), which optimizes the fit by minimizing the sum of squares of error (SSE). The Marquardt algorithm is an iterative routine that systematically adjusts the values of each unknown parameter "B" based on the value of $\partial(SSE)/\partial B$ in the current iteration.

For the curve-fitting we must let the least-squares algorithm compare predicted output voltage (i.e., the voltage calculated from theory for some postulated value of R_0) with measured output voltage, whereas equation [A3] tells us only the amplitude of sound waves radiated from a bubble of a given size. Equation [A3] must therefore be combined with the equations describing the bubble detector's operating characteristics. How that will be done is described below.

We will have measured values of the $|V_{out}{}^{2h}|$, the amplitude of the 2nd harmonic component of the output voltage. We also can compute a theoretical value of $|V_{out}{}^{2h}|$ from the theoretical amplitude of sound pressure received from the bubble according to the following equation:

$$|V_{out}{}^{2h}| = |P_{rad}{}^{2h}| \; k_2/k_{out} \qquad [1]$$

where $|P_{rad}{}^{2h}|$ = amplitude of the 2nd harmonic component of the sound pressure radiated from the bubble, atm;

k_{out} = gain coefficient of the receiving pressure transducer, atm/V;

k_2 = gain coefficient of the circuitry in the output signal path, dimensionless.

Equation [A3] relates the theoretical $|P_{rad}^{2h}|$ to the bubble size. It is a complicated nonlinear function that will be given a shorthand representation here:

$$|P_{rad}^{2h}| = f(\ |P_{in}|,\ R_0,\ n_{bub},\ f_d,\ d,\ \ldots\ ) \qquad [2]$$

where $|P_{in}|$ = amplitude of the externally applied sound, atm;

R_0 = equilibrium bubble radius, cm;

n_{bub} = number of bubbles;

f_d = driving frequency, Hz;

d = distance between bubbles and transducer head, cm.

The amplitude $|P_{in}|$ of the driving signal is rewritten in terms of the voltage sent to the transmit pressure transducer:

$$|P_{in}| = k_{in}\ |V_{in}| \qquad [3]$$

where k_{in} = gain coefficient of the transmit transducer k_{in}, atm/V;

$|V_{in}|$ = input voltage amplitude, V.

The input voltage is given in turn by

$$|V_{in}| = |V_{gen}|\ k_1 \qquad [4]$$

where $|V_{gen}|$ = output voltage amplitude from the signal generator, V;

k_1 = overall gain coefficient for the circuitry between the signal generator and the transmitter, dimensionless.

The input pressure amplitude that should be substituted into equation [2] is now seen to be $|P_{in}| = k_{in}\ k_1\ |V_{gen}|$. Given that the factors $(k_{in}\ k_1)$ and (k_{out}/k_2) are known, we see that the predicted $|V_{out}^{2h}|$ can be calculated from equation [1] for any given values of bubble radius R_0 and bubble number n_{bub}.

The least-squares algorithm compares the predicted $|V_{out}^{2h}|$ from equation [1] with the measured $|V_{out}^{2h}|$. It systematically adjusts the values of R_0 and n_{bub} to improve the goodness-of-fit of model to data, that is, to bring the predicted $|V_{out}^{2h}|$ into better agreement with the measured $|V_{out}^{2h}|$.

The factors (k_{in} k_1) and (k_{out}/k_2) are frequency-dependent and must be measured against a National Institute of Standards and Technology (NIST) standard. Beaming plots, which show the sound pressure level in front of the transducers as a function of position along the axial and radial axes, also will be obtained by measurement against NIST reference standards.

PRINCIPLES OF OPERATION

Figure 2a is a circuit diagram of the bubble detector. In Figures 2b and 2c, the frequency components present in the voltage signal at various stages in the bubble detector circuitry are indicated on this same circuit diagram. Figure 2b is drawn for the case in which the fundamental component of the backscattered sound is to be investigated, whereas Figure 2c is drawn for the case in which the second harmonic component is of interest.

The two ceramic piezoelectric pressure transducers are identical. Each has a semicircular head and the two are mounted side-by-side to form an approximately circular head of about 2.3 cm in diameter. The transmit transducer is designed to generate approximately planar sound waves. Each transducer is canted inward so that they focus on a point 3 - 3.5 cm from the transducer head.

The signal generator sends a swept-frequency voltage signal to the signal splitter, from which one part of the signal is routed to the transmit pressure transducer and the other part goes to the signal mixer. The portion going to the transmitter can be sent through a circuit that divides its frequency by 2, as shown in Figure 2c; this divider circuit is used when one wants to study the second harmonic component of the backscattered energy, and is bypassed when one is interested in the fundamental component. The sweep rate must be constant, for reasons which will become evident shortly. Experiments to date have been performed with the signal generator set to provide a 1.0V RMS signal sweeping from 0.2 to 5 MHz over a 0.1-second time span, which translates into a 48 MHz/s sweep rate. The sweep rate and frequency range are adjustable; the chosen frequency range roughly corresponds to the operating range of the transducers.

The signal from the receive transducer is amplified and sent to the mixer. The mixer's function is to multiply together the signals fed to it, generating "sum frequency" and "difference frequency" signals according to the following trigonometric identity:

$$\sin(a)\sin(b) = 1/2\ [\cos(a-b) - \cos(a+b)] \qquad [5]$$

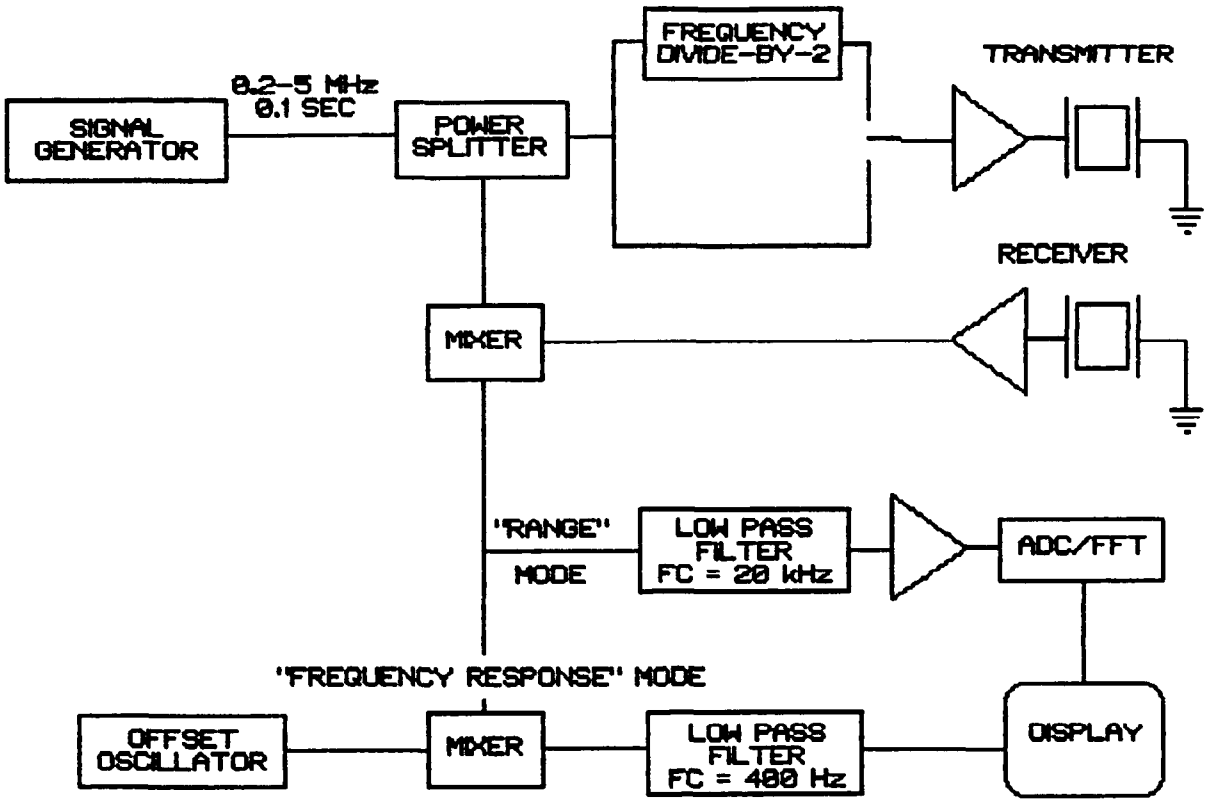

Figure 2a: Diagram of bubble detector system

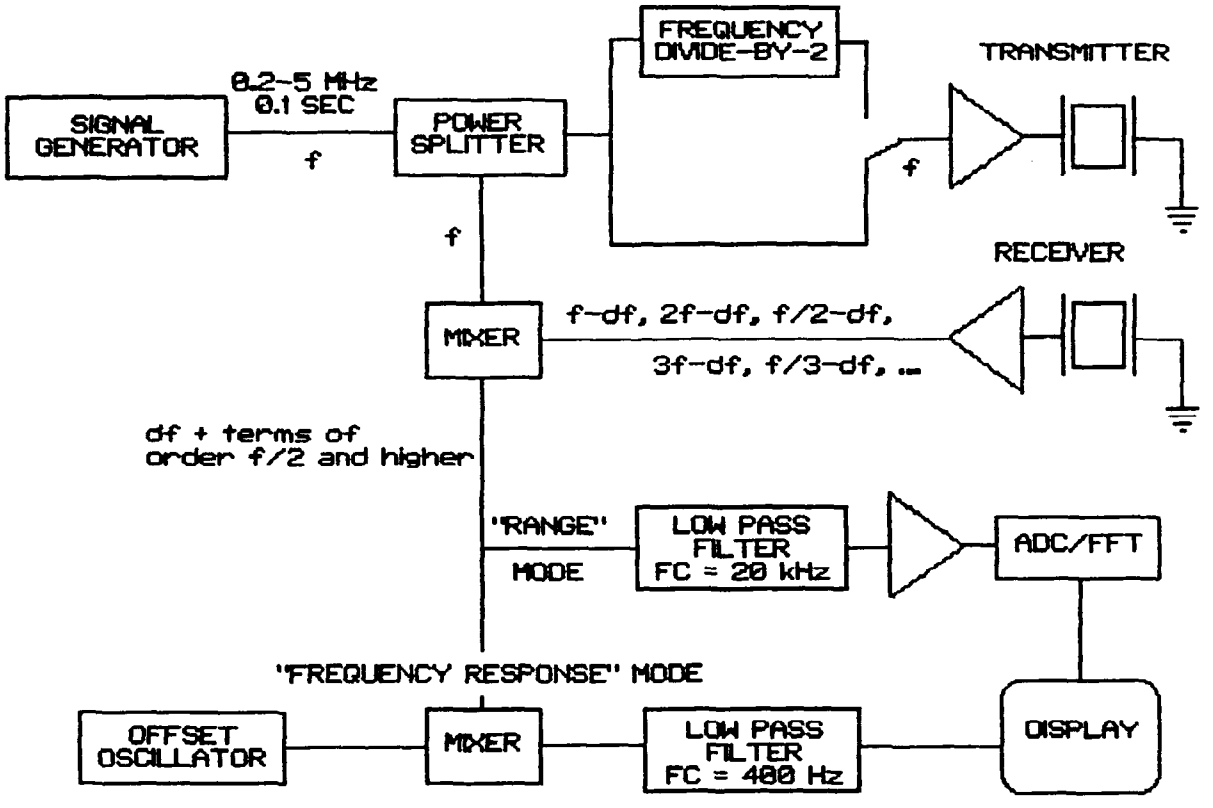

Figure 2b: Diagram of bubble detector system showing the signal frequencies at key points in the signal path: divide-by-2 circuit bypassed

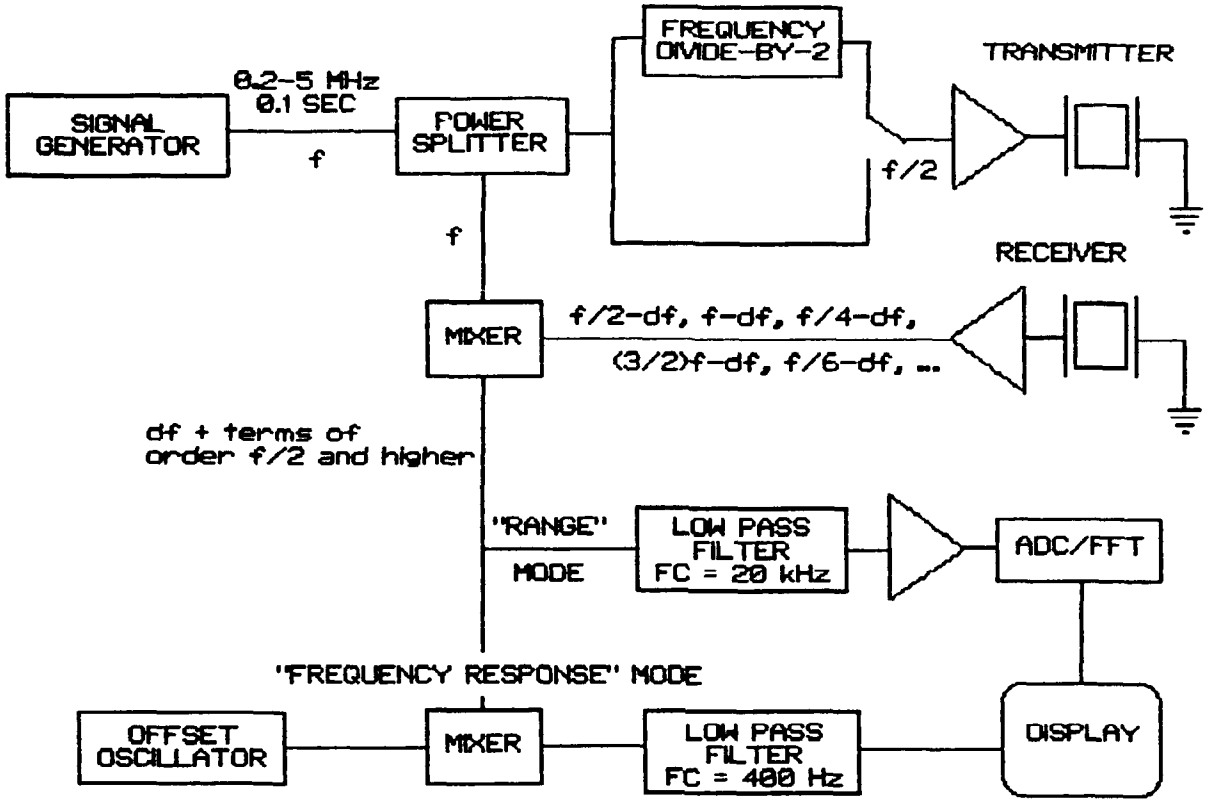

Figure 2c: Diagram of bubble detector system showing the signal frequencies at key points in the signal path: divide-by-2 circuit in use

Phase differences between the mixer's input signals affect neither the frequency nor the amplitude of the output signal. We now consider what the sum and difference frequencies should be in the signal exiting the mixer.

If the "divide-by-2" circuit has been bypassed, then Figure 3a shows the time-dependence of the frequencies of 1) the originally generated signal and 2) the fundamental component of the signal coming from the receive transducer if only one stationary target is present to backscattter energy. The time delay Δt required for sound to travel to the target and back again is seen to translate into a frequency offset Δf between the driving signal and the backscattered signal. This offset is constant throughout the sweep because the sweep rate is constant. An inspection of Figure 3a shows one how to calculate the frequency offset:

$$\Delta f = 2(\text{target distance})(\text{sweep rate})/(\text{velocity of sound}) \quad [6]$$

Remember that this is the correct frequency offset only for the fundamental component; other frequency components have greater offsets that change during the sweep. This point will be discussed shortly. Figure 2b shows the frequency components that are present in the signals entering and leaving the mixer when the "divide-by-2" circuit is bypassed.

If the divide-by-2 circuit has been employed, then Figure 3b represents the time-dependence of the frequencies of 1) the originally generated signal, 2) the signal to the transmitter, and 3) the second harmonic component of the signal from the receive transducer (again assuming for simplicity that only one stationary target is present). Once again we discover a time-invariant frequency offset between the signals entering the mixer, and again its value is given by equation [6]. Observing Figure 2c, notice that the frequency range of the transmitted signal is 0.1 to 2.5 MHz when the divide-by-2 circuit is used.

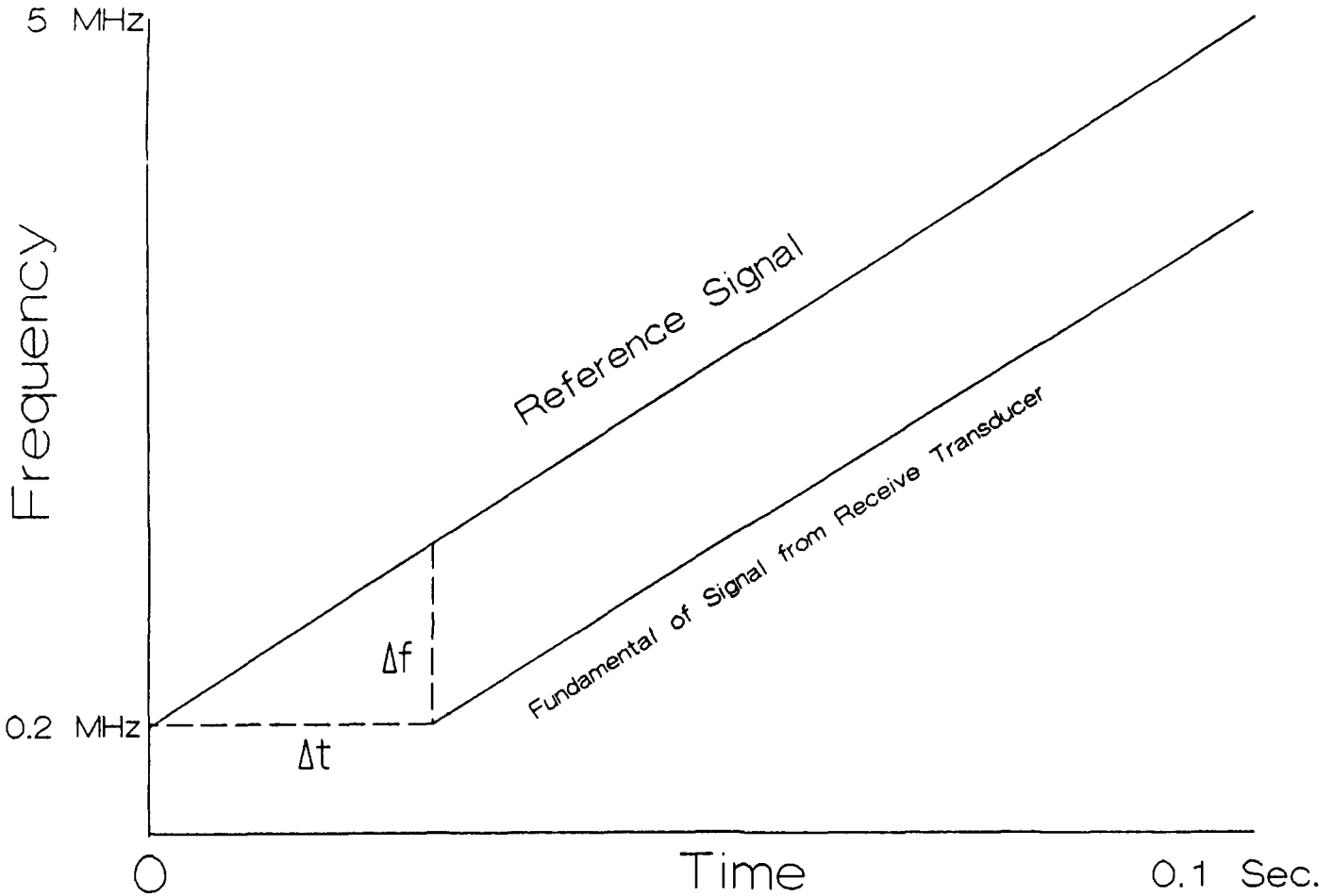

FIGURE 3A: ILLUSTRATION OF OFFSET FREQUENCY; "DIVIDE-BY-2" CIRCUIT BYPASSED

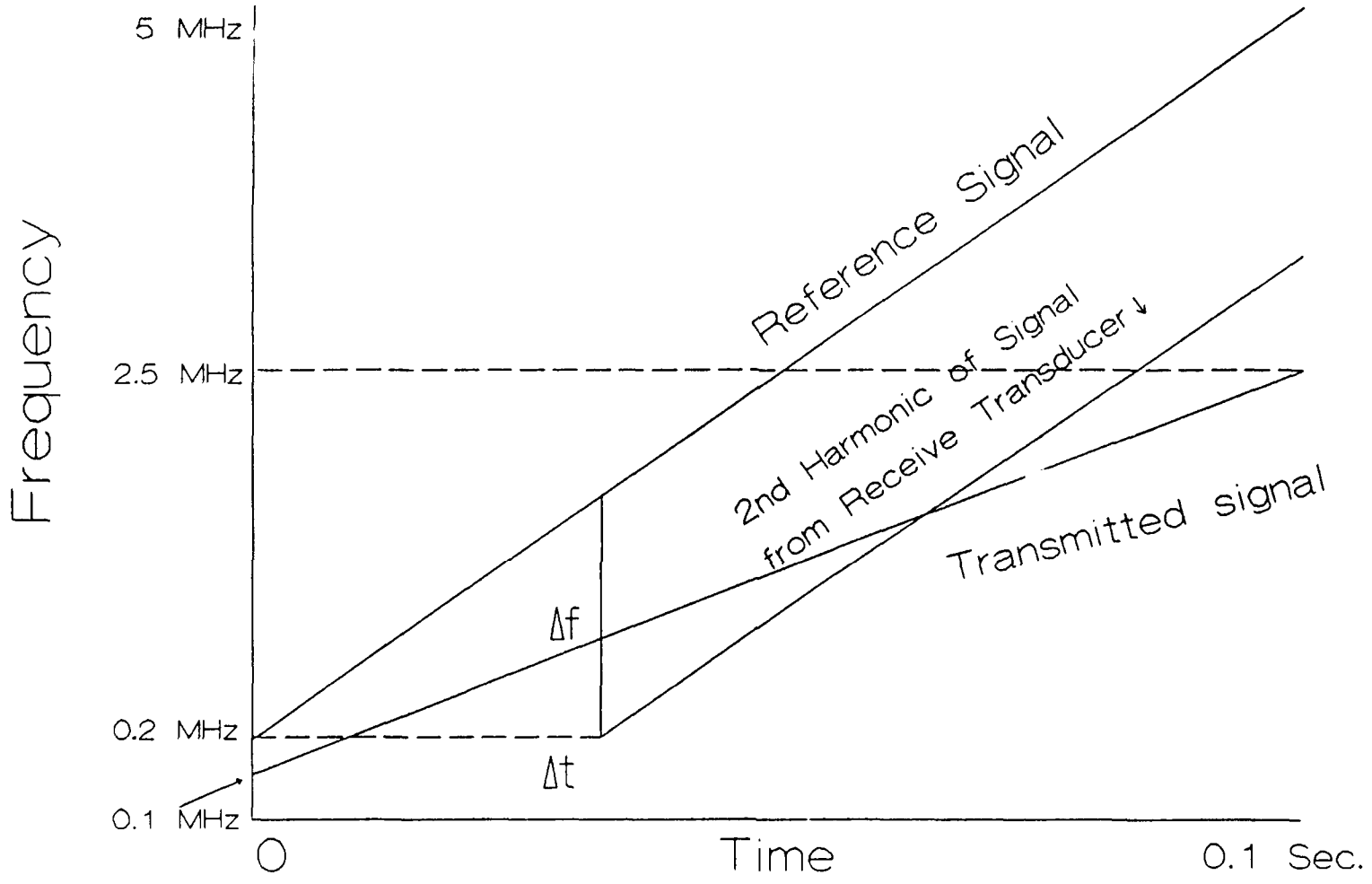

FIGURE 3B: ILLUSTRATION OF OFFSET FREQUENCY; "DIVIDE-BY-2" CIRCUIT IN USE

Multiplying two signals that differ in frequency by an amount Δf generates a signal having two components, one of which is of frequency Δf, as seen by rewriting equation [5]:

$$A\sin[2\pi ft]\ B\sin[2\pi(f+\Delta f)t] =$$
$$0.5AB\ \{\ \cos[2\pi\Delta ft]\ -\ \cos[2\pi(2f+\Delta f)t] \qquad [7]$$

So, we see that Δf is the frequency of one of the difference signals generated by the mixer. The strength of the signal leaving the mixer is determined by the conservation of power and current:

$$V_{out} = (V_1 \cdot I_1 + V_2 \cdot I_2)/(I_1 + I_2) \qquad [8]$$

where V_1, V_2, I_1, and I_2 are the voltages and currents of the two signals entering the mixer.

The value of Δf is a few kHz when water is the medium of sound propagation between the transducers and the target. For instance, for a target distance of 3.25 cm and a sweep rate of 48 MHz/sec the offset is 2.1 kHz. All other sum and difference signals generated by the mixer have frequencies on the order of at least 50 kHz. To understand this, recall from the section on "Gas Bubble Oscillations" that the signal backscattered from the target contains multiple frequencies. If the transmitted frequency is f, then the return signal contains components of frequency f, f/2, 2f, f/3, 3f, etc. By the time a backscattered signal arrives at the receive transducer, the reference signal has increased in frequency by an amount Δf. The mixer generates an output signal having two frequency components for each frequency present in the received signal, as shown in the following example for a reference signal of frequency f:

frequency component in the received signal	difference component and sum component in the mixer's output signal
f	Δf , $(2f + \Delta f)$
2f	$(f - \Delta f)$, $(3f + \Delta f)$
f/2	$(f/2 + \Delta f)$, $(3f/2 + \Delta f)$
3f	$(2f - \Delta f)$, $(4f + \Delta f)$
f/3	$(2f/3 + \Delta f)$, $(4f/3 + \Delta f)$

We see that, by far, the lowest frequency present in the mixer's output is Δf, which is the difference signal obtained by multiplying the reference signal with the received component of frequency f. We also note that the Δf component is the only one whose frequency remains constant as f varies during the sweep. The other frequencies in the mixer output are of order f/2 or greater. For a transmitted signal ranging from 0.1 to 2.5 MHz this means that the second lowest frequency present in the mixer's output varies from about 50 kHz to about 1.25 MHz during the sweep.

Essentially, the mixer is generating a single "intermediate frequency" (in the kHz range) tone of constant frequency Δf for each target, along with a number of "radio frequency" (in the MHz range) tones. The signal path from this point on depends upon which operating mode has been selected.

Range Mode

The "range" mode is useful for determining the distances of interesting targets from the transducer heads. In this mode, the mixer's output signal is sent through a low-pass filter with a 3dB point of 20 kHz, eliminating all signal components except for the Δf component. Therefore, all frequency components in the signal captured by the receive transducer have been filtered out, except for either the fundamental or the second harmonic (depending on whether the divide-by-2 circuit was used). The signal at this point consists of one tone of constant pitch for each target. These tones are amplitude-modulated (AM) because, in general, the amount of energy backscattered from a target depends on the driving frequency, which in turn is a linear function of time. The signal is passed through an analogue-to-digital converter (ADC) and is then Fourier transformed, and the output is an amplitude spectrum. There is one amplitude peak at each offset frequency Δf corresponding to each target distance. Fourier transformation of AM signals causes one to lose time-domain information because the FFT must be done over a finite time interval and consequently there is an averaging of the amplitudes over that interval (in this case the time record encompasses the entire

0.1 sec sweep time). However, this is not serious since the range mode is used only to locate targets.

Note that Fourier-transforming the signal over the time of an entire sweep is practical only because the system has succeeded, via the mixing and filtering, in reducing radio frequency signals to intermediate frequency signals. Without this frequency reduction the necessary sampling rate would be orders of magnitude higher, requiring in turn a prohibitively large storage space for digital samples.

Frequency Response Mode

The more critical operating mode is the "frequency response" or "FRC" mode, in which time domain information is obtained for targets at some selected distance from the transducer head. From this information we can, in principle, deduce the sizes and numbers of bubbles in a sample. The components in the FRC signal path constitute an AM tuner; they 1) sort out a number of AM signals and discard the unwanted ones, keeping only those whose frequencies fall within a narrow passband, and 2) de-modulate the signals of interest. In the design of the current system, the signal path in this mode contains only analogue signal processors.

The offset oscillator (see Figure 2) is tuned to the offset frequency Δf corresponding to the target distance of interest, and it generates a signal of constant amplitude and frequency. (The range mode can be used to determine the offset frequencies of interesting targets prior to tuning the oscillator). The mixer multiplies the AM signal coming from the first mixer with the signal from the oscillator. The mixer's output includes some difference frequency components of only a few Hz -- these arise from the targets at distances such that Δf is close to the frequency to which the oscillator is tuned. The signal is low-pass filtered again, the filter this time having a 3 dB point at 400 Hz and a steep 30 dB/octave rolloff. The remaining signal is an amplitude-modulated voltage containing frequencies of up to 400 Hz; its amplitude at any time instant is a function of the amplitude of either the fundamental component or the second harmonic component (depending on whether

the divide-by-2 circuit is in use) of the sound backscattered from targets at some certain distance from the transducer head. This amplitude-vs-time plot is readily converted to an amplitude-vs-driving frequency spectrum. This is the desired output; the "Data Handling" section explains how data-fitting by SSE minimization is applied to these data.

The sample thickness that is being interrogated in the FRC mode is determined by the cutoff frequency of the low-pass filter. The one supplied by JPL has a 400-Hz cutoff, meaning that the filter passes any signal from a target having a Δf within 400 Hz of the frequency to which the oscillator is tuned. Equation [6] shows that this 800-Hz passband translates into a thickness of 1.25 cm.

PREPARATION AND EXAMINATION OF HYDROGEL SAMPLES

For calibrating the bubble detector, it is necessary that we have standards for which numbers, sizes, and locations of bubbles can be determined by some reliable independent method. The bubble detector currently has no provision for accessing the numerical data or transferring data to any other device, so that quantitative experimentation is not yet possible and calibration is precluded pending modification of the hardware. In the meantime, we have prepared bubble samples of the sort we anticipate using as calibrants and used them in some preliminary measurements intended to estimate the bubble detector's signal/noise ratio. In this section we describe a protocol for preparing and examining calibration standards.

We plan to use calibrants consisting of bubbles trapped in transparent hydrogels and we plan to assay them using differential interference microscopy at a magnification of at least 500X. For simplicity, in these preliminary trials the hydrogels were examined using a bright field microscope at only 100X, calibration being impossible as yet. At this magnification, one cannot accurately measure the sizes of objects having characteristic lengths of less than 10 or 20 μm, so the bubbles which the system was designed to detect could not be quantitatively assayed in these preliminary trials.

To produce the gels, aqueous solutions were prepared in the following compositions:

solution A:

0.20 g/ml acrylamide monomer

0.01 g/ml N,N'-methylene-bis-acrylamide crosslinking monomer

1.0 μl/ml N,N,N',N'-tetramethylethylenediamine accelerator

solution B:

variable 0.15-0.25 mg/ml ammonium persulfate initiator

Prior to mixing the solutions, each was sparged with nitrogen to remove dissolved oxygen, which inhibits many vinyl polymerizations (15). Each solution was passed through a filter having a 0.45-μm nominal pore size to remove particles that otherwise would severely confuse the microscopic

examination. Equal amounts of solutions "A" and "B" then were mixed and the resulting solution was cast between cleaned glass plates. To make thin gels, the plates were separated by a shim of waxed paper of 60-μm thickness. For thick gels, the plates were separated by 1.5-mm-thick Teflon spacers designed for use in casting electrophoresis gels. The glass plates, with monomer solution sandwiched between them, were placed in a vacuum for several minutes (no fixed length of time). The polymerization was then allowed to proceed at ambient pressure at least until gelation occurred. Bubbles that formed by cavitation at the reduced pressure were trapped in the finished gel.

In order to be useful, the calibration standards must be the same size when they are interrogated ultrasonically as when they were assayed microscopically. Accordingly, the stability of these bubbles over time was tested by examining some of them over several days' time while leaving the gel membrane sandwiched between the glass plates. The sizes of gas bubbles trapped in polyacrylamide gels were seen generally to be stable over a period of 4 days. The exceptions were bubbles near the edges of the gel, which often disappeared. The reason for this may be that these gels were stored in open air rather than in a humidified environment, so that desiccation around the edges might be expected (remember that these gels were stored between the glass plates so that their edges alone were exposed to air). Desiccation causes the collapse of small cavities in hydrogels. The actual calibration standards will be assayed microscopically and interrogated by the bubble detector within 24 h of their production. They will be stored in a humid atmosphere.

To provide samples for interrogation by the bubble detector, the finished gels were prevented from dehydrating by storing them in an enclosed container whose interior was kept at the dew point by the presence of standing water. Any portion of a gel membrane that was seen upon microscopic examination to contain one or more bubbles was cut out and mounted on a slab of Wall-Gone sound absorbent rubber (to reduce background reflection of the transmitted sound) and was positioned in front of the transducer head. The Wall-Gone,

target, and transducer head were immersed in water during interrogation because impedence differences at the gas-solid interface precludes the transmission of ultrasound through air.

PRELIMINARY TRIALS WITH THE JPL BUBBLE DETECTOR

This section is a summary of the results of the preliminary experiments with the bubble detector. The goal of most of these experiments was to estimate the system's signal/noise ratio.

Measuring the Velocity of Sound (Range Mode)

With the range mode selected for display, sound was reflected off of a flat metal target located at various distances from the transducer head and equation [2] was used to compute the velocity of sound in water from the offset frequency of the voltage peak representing the reflected sound. The displayed voltage amplitude spectrum actually contained a number of peaks, at offset frequencies of Δf, $2\Delta f$, $3\Delta f$, etc., with peaks getting progressively smaller at higher frequencies. The extra peaks represent sound that was reflected back and forth more than once between the target surface and the transducer head. The value of Δf for use in equation [2] was taken as the frequency at which the first peak was at its maximum. The calculated velocity was $1.40 \cdot 10^5$ cm/sec with a standard deviation of $0.023 \cdot 10^5$ cm/sec for $n = 8$ measurements. The handbook value for sound in water at 20°C is a bit higher at $1.486 \cdot 10^5$ cm/sec, possibly suggesting that Δf should have been taken as the frequency at which the edge of the first peak appeared, rather than the frequency at which its maximum occurred.

Measuring the Signal/Noise Ratio

We attempted to quantify the amount of electronic noise generated by various noise sources. Noise measurements were made using signal averaging over several minutes time. Of primary interest is the amount of noise present in the FRC output when the divide-by-2 circuit is in use, because this is the output from which we hope to deduce bubble sizes by analyzing the 2nd harmonic component of the sound radiated from bubbles.

I. Range Mode:

The noise observed in the range mode output represents the combined noise from all processing stages except those unique to the FRC mode (see Figure 2). In the range mode the baseline noise was less than 0.1 mV regardless of

whether the fundamental or the second harmonic frequency component was on display (i.e., whether the divide-by-2 circuit was in use). The noise did not appear to depend on offset frequency. It is doubtful that the digitizer or the FFT contributed significantly to the noise level. A DC component was always present in the range mode's output. This represents a signal received with no time delay at all, and it must result from crosstalk between the transducers. It would only be mistaken for a bubble if the operator expected a bubble to be present at the transducer surface.

II. Frequency Response Mode:

In the remainder of the experiments to be reported on, the frequency response (FRC) mode was used. Whereas the bubble detector presently has no provision for accessing the numerical data, we had limited means of analyzing the data from these experiments. The current system does display amplitude spectra on a VDT screen. Therefore, to characterize the system's output in the FRC mode we chose arbitrarily to record the maximum output voltage V_{max} as read from the graphs displayed in the FRC mode.

It would be quite difficult to elucidate the physical significance of V_{max}. The FRC output consists of a group of amplitude-modulated waveforms summed together. The frequencies of the individual waveforms are anywhere between 0 and 400 Hz, because the output signal is sent through a low-pass filter having a cutoff frequency of 400 Hz. The V_{max} occurs when the sum of the waveforms happens to be at its maximum. This depends on the target distances and the frequency to which the offset oscillator is tuned, because these factors determine the frequencies of the waveforms that constitute the FRC output signal. Our use of V_{max} to characterize the FRC data is seen to be a crude technique, but nevertheless it allowed us to make some important observations of the system's performance, the discussion of which will occupy the rest of this section.

To measure the noise generated by components in the FRC mode's circuitry, we used the bubble detector to interrogate a bubble-free region in a water tank. We detuned the offset oscillator away from any offset frequency

corresponding to the distance of any visible target and recorded the V_{max} displayed in the FRC mode. V_{max} was found to depend on the amplitude of the offset oscillator's signal, which is adjustable. With the divide-by-2 circuit in use, the measured V_{max} increased monotonically from 1.5 mV to 8 mV as the oscillator gain setting was increased from 10 to 1000. The gain setting is written in arbitrary units. Without the divide-by-2 circuit, V_{max} increased from 1.8 mV to 36 mV as the gain was increased from 10 to 1000. Note that the output voltage V_{out} in the FRC mode is itself a function of the oscillator's gain setting (see equation [4]), so that whereas the noise level is elevated by increasing the gain, the signal/noise ratio is not necessarily degraded.

The supposed source of this noise is interference by the offset oscillator with the wiring between the two signal mixers. In other words, voltage leakage from the offset oscillator induces a current that matches the frequency of the oscillator's signal, so that the signal multiplication produces a DC component which then passes through the low-pass filter and becomes part of the output. A spectral analysis of the FRC output shows that there is indeed a DC component whose magnitude does not seem to depend on what frequency the oscillator is tuned to. This explanation accounts for the correlation between the noise level and the oscillator's gain setting, but we have no explanation as yet of why the noise is greater with the divide-by-2 circuit bypassed than when it is in the signal path.

Another noise source when one is studying the second harmonic is the nonlinearity of the transducers themselves. The transmitted sound contains a second harmonic component that is generated by the transmit transducer. Part of this component is reflected from any solid target and captured by the receive transducer, and shows up as a spurious bubble. The magnitude of this noise depends of course on how reflective is the target or medium near the target. In addition, the fundamental component of the received sound is partly converted to a second harmonic signal owing to the nonlinearity of the receive transducer. In the FRC mode, the observed magnitude of noise arising

from transducer nonlinearities depends on the gain setting on the offset oscillator.

The magnitude of this noise can be estimated only with the divide-by-2 circuit in use. When a slab of Wall-Gone sound absorbent rubber at a distance of 3.25 cm was used as the target, the maximum (signal-averaged) voltage in the FRC mode was increased from 2.0 mV at a gain setting of 10, to 27 mV at gain = 1000. Keep in mind that these noise levels contain contributions from both of the noise sources mentioned previously; they are measurements of total noise.

We expect that the amplitude ratio of the second harmonic component to the fundamental in the transducer response is frequency-dependent. In particular, nonlinearities should be maximized near the resonance frequency, and these transducers are swept through their resonance frequency during a 0.2-to-5-MHz sweep. We presently have no way to quantify the nonlinearity of each transducer independently.

To interrogate hydrogel targets, we used the FRC mode with the divide-by-2 circuit in use so that the output voltage was a function of the second harmonic component of the received sound (this is the configuration that is potentially useful for determining bubble sizes). The offset oscillator was set arbitrarily at gain = 100 for all of the hydrogel experiments. At this setting we measured V_{max} = 7.5 mV when the transmitted sound was simply reflected from the slab of Wall-Gone; this is a measure of the total noise at the second harmonic frequency at gain setting = 100. The hydrogel membranes were mounted on Wall-Gone at a distance of 3.25 cm from the transducer head.

We first experimented with poly-acrylamide membranes that had been prepared without decompressing the monomer solution, which therefore should not contain bubbles. Microscopic inspection of the 60-μm-thick samples confirmed that they were bubble-free. Because the gels' thickness (1.5 mm) was greater than the focal length of the objective lens on our microscope, the visual scan done on them was incomplete. The presumption is that these thicker gels were also bubble-free or at least contained very few bubbles.

The measured V_{max} in the FRC mode was found to be essentially the same as in the absence of any gel, so that there was no indication that the polymer itself significantly affected V_{max}. For the thin membranes, V_{max} averaged 7.6 mV with a standard deviation of 1.7 mV for n = 7 samples. For the thick membranes V_{max} = 8.1 mV and S.D. = 1.4 mV for n = 8. An incidental observation is that when the 1.5-mm-thick membranes were interrogated in the range mode, two separate peaks could be discerned at offset frequencies corresponding to both the front surface of the gel and the interface between its rear surface and the Wall-Gone mounting. For the thin gels the difference between these offset frequencies was too small to permit the distinction of separate peaks.

For the 60-μm-thick bubble-bearing membranes the average measured V_{max} was 12.6 mV with a standard deviation of 2.6 mV. This is higher than what was measured for the non-bubbled membranes, though the difference is not statistically significant at the $p<0.05$ level. The output voltage was significantly higher for the 1.5-mm-thick, bubble-bearing membranes: V_{max} averaged 33 mV with S.D. = 12 mV.

CONCLUSIONS AND RECOMMENDATIONS

During our interrogations of hydrogels, we were able to measure a significantly higher output voltage at the second harmonic frequency for 1.5-mm-thick bubble-bearing membranes than for membranes without bubbles. Thinner membranes containing bubbles did not yield a significantly higher output voltage, presumably because they contained fewer total bubbles. Therefore, we can say that the bubble detector, as designed and delivered, appears to enable the investigator to distinguish qualitatively between the presence and absence of bubbles, given that the bubbles are numerous enough to produce a sufficiently strong output signal.

However, the system also suffers from some conspicuous shortcomings, and it is not going to yield any useful quantitative data until they are corrected. First, it allows no access to its numerical output. Therefore, an A/D converter that can be interfaced with a programmable computer should be installed to digitize the analogue signal from the bubble detector and send it where it can be stored for later manipulation.

Second, the signal/noise ratio is far too low; but this problem can be reduced if not eliminated. Much of the noise in the FRC mode is generated by the offset oscillator, mixer, and low-pass filter. As we have seen, they function as an AM tuner. It would be desirable to replace them with a digital AM tuner. Such a device would combine digital de-modulation with digital filtering and would function almost noise-free by dispensing with analogue steps. We currently are exploring whether a suitable machine of this sort is available.

The other major noise source is a consequence of the nonlinear response of the transducers, and this is not readily correctable. Signal averaging must be used to ameliorate the problem via a subtraction of the time-averaged noise from the time-averaged sum of signal and noise.

When the S/N ratio has been improved as much as is practical, then we must evaluate whether it has improved enough that we can get quantitative information on individual bubbles. One way to make this evaluation is as

follows: After the gain coefficients of the transducers have been measured and the equations describing bubble oscillations have been encoded in a computer program, then it will be possible to predict, for a given input voltage, the sound pressure incident to a bubble, the sound pressure re-radiated by the bubble to the receive transducer, and the output voltage from the receive transducer. In other words, we can use equation [4] to compute a theoretical V_{out} after 1) generating theoretical values of P_{rad} using the methods summarized in the Appendix and 2) empirically determining the gain coefficients k_2 and k_{out}.

If the S/N ratio is not adequate for studying individual bubbles, then two alternatives come to mind. First, use of the system could be limited to the analysis of dense populations of small bubbles. The functions to be fitted to data would need to be altered by the addition of parameters that characterize population statistics.

Second, we could choose to study larger bubbles, thus exploiting the fact that, to a first approximation, the energy radiated from an oscillating bubble is proportional to the cube of its radius. This is a way of increasing the S/N ratio without improving any electronic components. This approach would require that we replace the existing transducers with a pair designed for a lower frequency range, which would encompass the resonance frequencies of larger bubbles. The size range of bubbles that are relevant to DCS is unknown, so there is no reason to insist upon studying bubbles of any particular size range so long as the size is physiologically plausible.

REFERENCES

1. Nyborg W.L., "Physical principles of ultrasound." In: Fry F.J. (ed.), Ultrasound: Its Application in Medicine and Biology. New York: Elsevier, 1978.
2. Prosperetti A., "Nonlinear oscillations of gas bubbles in liquids: steady-state solutions." Journal of the Acoustical Society of America, Vol. 56, pp. 878-885, 1974.
3. Prosperetti A., "Thermal effects and damping mechanisms in the forced radial oscillations of gas bubbles in liquids." Journal of the Acoustical Society of America, Vol. 61, pp. 17-27, 1977.
4. Miller D.L., "Ultrasonic detection of resonant cavitation bubbles in a flow tube by their second-harmonic emissions." Ultrasonics, Vol. 19, pp. 217-224, 1981.
5. Vacher M., Gimenez G., and Goute R., "Nonlinear behavior of microbubbles: Application to their ultrasonic detection", Acustica, Vol. 54, pp. 275-283, 1984.
6. Christman C.L., Catron P.W., Flynn E.T., and Weathersby P.K., "In vivo microbubble detection in decompression sickness using a second harmonic resonant bubble detector." Undersea Biomedical Research, Vol. 13, pp. 1-18, 1986.
7. Prosperetti A., "Nonlinear oscillations of gas bubbles in liquids: Transient solutions and the connection between subharmonic signal and cavitation." Journal of the Acoustical Society of America, Vol. 57, pp. 810-821, 1975.
8. Prosperetti A., "Nonlinear bubble dynamics." Journal of the Acoustical Society of America, Vol. 83, pp. 502-514, 1988.
9. Prosperetti A., "Numerical integration Methods in gas-bubble dynamics." Journal of the Acoustical Society of America, Vol. 85, pp. 1538-1548, 1989.
10. Achenbach J.D., "Wave propagation in elastic solids." New York: Elsevier, 1973.

11. Jackson E. Atlee, "Perspectives of nonlinear dynamics." Cambridge Press, Cambridge, U.K., 1989.

12. Lautherborn W., "Numerical investigation of nonlinear oscillations of gas bubbles in liquids." Journal of the Acoustical Society of America, Vol. 59, 283-293 (1976).

13. Crum L.A. and Prosperetti A., "Nonlinear oscillations of gas bubbles in liquids: An interpretation of some experimental results." Journal of the Acoustical Society of America, Vol. 73, pp. 1-127, 1983.

14. Marquardt D.W., "An algorithm for least-squares estimation of nonlinear parameters." Journal of the Society of Industrial Applied Mathematics, Vol. 11, pp. 431-441, 1963.

15. Flory P.J., "Principles of polymer chemistry." New York: Cornell University Press, 1953.

APPENDIX: MATHEMATICAL BACKGROUND

1. Introduction

Most of the mathematical analysis in this report revolves around an ordinary differential equation that describes the oscillations of a bubble in a liquid caused by an incident sound wave. Last century, Lord Rayleigh derived the equation of motion for the medium surrounding a spherical bubble when the ambient pressure oscillates sinusoidally about its mean. Like many basic equations in physics that describe the behavior of fluids, Rayleigh's equation is a non-linear differential equation that is very difficult to solve. Over the years mathematicians have developed several methods for finding approximate solutions to nonlinear differential equations, in particular those that represent nonlinear harmonically driven oscillators. In recent decades, several engineers have found approximate solutions to Rayleigh's equation by using an averaging method developed, beginning in the 1930's, by the Russian mathematicians Krylov, Bogolyubov, and Mitropolsky (reference A1).

In order to apply most nonlinear methods (including the Krylov-Bogolyubov-Mitropolsky) it is necessary to make some simplifying assumptions. Even with appropriate assumptions, the calculations can be quite involved. Estimation of parameters may require use of additional equations. Before describing assumptions and parameters for the bubble equations, we will provide an overview of the theory of solutions to nonlinear forced oscillator equations. The general results from the theory allow one to better understand the special results achieved for Rayleigh's equation and the necessity of certain simplifying assumptions that allow the theory to be applied.

2. Basic Facts about Solutions to Nonlinear Forced Oscillator Equations

Consider nonlinear oscillator equations of the form

$$x'' + \omega_0^2 x = \epsilon f(x,x') + \epsilon A \cos(\omega t) \qquad (x' = dx/dt)$$

where 'x' represents the displacement from equilibrium, $\epsilon f(x,x')$ represents all the nonlinear damping and restoring force terms, and $\epsilon A \cos(\omega t)$ represents

the forcing (or driving) function. The 'ϵ' denotes a small perturbation parameter; thus the nonlinear damping and restoring force terms as well as the forcing function are assumed to be small compared with the two terms on the left-hand side. The parameter 'ω' is called the driving frequency and ω_0 is called the natural frequency (of the oscillator).

The theory of such equations (references A1, A2) shows that they often have resonance solutions; i.e., a solution that, when expressed in terms of the parameter 'ω', has an amplitude that grows sharply as 'ω' approaches certain special values called resonance frequencies. Unlike linear equations, nonlinear equations often have two or more stable solutions when 'ω' is close to a resonance frequency. The resonance frequencies in general occur when 'ω' and 'ω_0' are related in one of the following ways:

If $\omega_0 = n\omega$ for some positive integer 'n', a solution with frequency ω_0 is called **(ultra)harmonic** (and the corresponding resonance frequency is ω_0/n);

If $\omega_0 = \omega/n$ for some positive integer 'n', a solution with frequency ω_0 is called **subharmonic** (and the corresponding resonance frequency is $n\omega_0$);

If $\omega_0 = m\omega/n$ for some integers $m,n > 1$, a solution with frequency ω_0 is called **ultrasubharmonic** (and the corresponding resonance frequency is $n\omega_0/m$).

In general when one resonance solution exists for a resonance frequency there will be <u>several</u> solutions of different amplitudes and with different phase shifts relative to the forcing function. All these solutions will be defined for some interval of ω-values near the resonance value. The number of solutions for the bubble equation is hard to predict since its $f(x,x')$ is complicated. With extensive computations it can be shown that there are three solutions for each of the following resonance frequencies: $\omega=\omega_0$ (main resonance solution), $\omega=\omega_0/n$ for $n = 2,3$ (ultraharmonic solutions), and $\omega=n\omega_0$ for $n = 2,3$ (subharmonic solutions). (Note: the existence of three solutions is based on the assumption that the driving and damping forces are weak relative to the restoring force of the bubble.)

The simplest example of a system with multiple resonance solutions is a pendulum with no damping that is harmonically driven. Its equation is

$$x'' + \omega_0^2 x - (1/6)\omega_0^2 x^3 = \epsilon A \cos(\omega t) \qquad \text{with } \omega = \omega_0 + O(\epsilon)$$

where $O(\epsilon)$ denotes a function of order ϵ (this implies 'ω' is close to ω_0). It can be shown that there will exist three solutions for some frequency interval just to the left of the main resonance frequency ω_0 (see reference A2, p. 126). The solutions have distinct amplitudes; the ones with the largest and smallest amplitudes are stable, whereas the solution with the intermediate amplitude is unstable. The solution with the largest amplitude is 180° out of phase with the forcing function; the other two solutions are in phase. All three solutions have finite amplitude for all values of 'ω' near ω_0, even though there is no damping (this contrasts with the linear pendulum). Because there are two stable solutions, the pendulum equation is called bistable and the set of solutions exhibits "hysteresis" (defined below).

Determining which stable resonance solution is achieved in an experiment depends not only on the driving frequency 'ω' but also on how that value of 'ω' is achieved experimentally. This is a special case of the general problem of determining which stable solution will be observed in a given experiment involving a nonlinear system when the system has two or more stable (and therefore observable) solutions.

If 'ω' is started above the resonance frequency (and is therefore to the right of the multiple solution region on the ω-axis) and is decreased gradually, then at the point where the three solutions come into existence the solution will take the upper track (i.e. the largest-amplitude solution will be observed) until the three solutions merge. At this point, a sudden decrease in the amplitude of the solution will be observed as the solution jumps down from the upper track to the single lower track. This is an example of the jump effect. (The formal term for jumps between stable solutions is "hysteresis"). Similarly, if 'ω' is started below the multiple solution region and is increased gradually it will take the lower track until there is only one track. This track will be higher and the solution will suddenly jump up to the largest-amplitude solution. Thus, there will be jumps observed whether the driving frequency is swept upward or downward; the downward jump

will in general be greater than the upward jump. The middle track, which is unstable, will not be observed in either an upward or downward frequency sweep. To fully understand these statements it is helpful to look at some hysteresis graphs (see Figure 1 in main report).

3. Mathematical Models Used in the Analysis of Bubble Oscillations

We will describe the major aspects of the derivation of the equation of motion for oscillations of a spherical bubble that is driven by a sinusoidal pressure field with a wavelength that is large compared to the bubble radius. There are three major steps: 1) calculating expressions for the effective viscosity, the polytropic exponent, and the natural frequency of a bubble system that reflect the fact that these parameters are functions of driving frequency, which requires using a variety of linearized equations described in reference [2]; 2) determining the set of resonance solutions for a low-order version of Rayleigh's equation which uses the frequency-dependent parameter expressions from step 1; and 3) showing how these resonance solutions are related to a quantity that the detector can measure, viz. the 2ω component of the radiated pressure wave from the bubble. (For details on step 1 see reference [3], on step 2 see reference [2], on step 3 see "Data Handling" in the main report.)

Step 1: A summary of Prosperetti's approach in reference [2] is as follows: He begins by expressing as an equation the boundary condition that the normal stresses are continuous across the bubble surface. Using a linearization of the "wave equation" (which is simply the equation of motion written for a compressible medium), the external pressure is written as the superposition of the contributions of the driving sound field and acoustic radiation from the bubble. The radiated pressure is calculated from the velocity potential for the liquid, which is determined by solving the linearized wave equation. The last major computation involves determining the internal pressure. This

requires the simultaneous solution of the linearized equations of mass and momentum in the gas and of energy both in the gas and in the liquid.

Let us now define the key variable and state assumptions regarding it. Define x(t) implicitly by

$$R(t) = R_0 \ (1 + x(t))$$

Thus x(t) represents the fractional radial deviation of the bubble radius R(t) from its equilibrium value R_0. We assume that x(t) and all its derivatives are small, i.e. much less than one, so that powers of x(t) and its derivatives higher than the first may be neglected.

All these results are combined to yield a single second order ordinary differential equation in x that has the form of a forced damped harmonic oscillator:

$$x'' + 2\beta\, x' + \Omega_0^2 x = -\epsilon\alpha\exp(i\ \Omega t)$$

The damping constant β is the sum of three particular damping constants termed viscous, thermal, and acoustic, i.e., $\beta = \beta_{vis} + \beta_{th} + \beta_{ac}$, where $\beta_{vis} = 2\mu/(\rho_L R_0^2)$, $\beta_{th} = 2\mu_{th}/(\rho_L R_0^2)$, $\beta_{ac} = 2\mu_{ac}/(\rho_L R_0^2)$. Here μ is the (ordinary) viscosity of the liquid, μ_{th} is the thermal viscosity, and μ_{ac} is the acoustic viscosity, which is defined by $.25(\rho_L\Omega^2 R_0^3/c)(1 + (\Omega R_0/c)^2)^{-1}$. The effective viscosity μ_{eff} is the sum of the ordinary, thermal, and acoustic viscosities. In the above, ρ_L denotes the density of the liquid, and c is the speed of sound (i.e. the pressure wave) in the liquid. The natural frequency Ω_0 is given by

$$\Omega_0^2 = 3k(P_{in,eq}/(\rho_L R_0^2)) - 2\sigma/(\rho_L R_0^3) + (\Omega R_0/c)^2(1 + (\omega R_0/c)^2)^{-1}\Omega^2$$

where k is the effective polytropic exponent, $P_{in,eq}$ is the internal pressure corresponding to R_0, and σ is the surface tension of the liquid.

The "effective polytropic exponent" k is defined for a gas in a container whose volume changes with time, as follows: let $P_{in}(t)$ be the internal pressure of the bubble, and V(t) its volume. Then if V_0 is the volume

corresponding to pressure P_0, the well-known pressure-volume law for compression (or expansion) of a gas can be expressed as $P_{in}(t)/P_0 = (V_0/V(t))^k$. During a compression (or expansion) heat may be exchanged between the bubble and the surrounding liquid. The extreme cases of zero and infinite heat transfer rates correspond to adiabatic and isothermal processes (respectively). For an isothermal compression it follows from the ideal gas law that $k = 1$. For an adiabatic compression, k has a value equal to the ratio of specific heats for the bubble gas. This ratio (specific heat at constant pressure to specific heat at constant volume) has been determined experimentally for various gases at various temperatures. For room temperature air it is about 1.4. It can be shown that, for either isothermal or adiabatic oscillations, the pressure and volume oscillations are exactly 180° out of phase.

However, for real processes (such as bubble oscillations) there is a finite, non-zero heat transfer rate that leads to a phase difference other than 180° between the pressure and volume variations. For oscillations, the polytropic exponent k will depend on this phase difference. This necessitates defining 'k' by the more general expression $P_{in} = P_{in,eq}\,(R_0/R(t))^{3k} - 4\mu_{th}x'$. After extensive computations, Prosperetti is able to show: $\mu_{th} = .25\Omega\rho_g R_0^2 \mathrm{Im}(\phi)$, $k = (1/3)(\Omega^2\rho_g R_0^2/P_{in,eq})\mathrm{Re}(\phi)$. Here ϕ is a complex quantity and $\mathrm{Im}(\phi)$ and $\mathrm{Re}(\phi)$ denote its imaginary and real parts, respectively.

The definition of ϕ is very involved; it depends on the molecular weight of the bubble gas, its thermal diffusivity, the ratio of the specific heats of the gas, the liquid temperature, the thermal diffusivity of the liquid, and the ratio of liquid to gas thermal conductivities (see reference [3] for details).

Step 2: In this step the Ω-dependent expressions for μ_{eff}, k, and Ω_0^2 determined in step 1 are substituted into the nonlinear bubble model expressed by Rayleigh's equation and the pressure-volume equation. Rayleigh's equation of motion for an incompressible Newtonian fluid surrounding a gas bubble is

$$RR'' + (3/2)\,(R')^2 = 1/\rho_L\,[P_{in}(t) - P(t) - 2\sigma/R - 4\mu_{eff}R'/R] \qquad [A1]$$

where $R = R(t)$ is the bubble radius at time t, $P_{in}(t)$ is the internal pressure at time t, and $P(t)$ is the ambient pressure at time t. We assume $P(t) = P_0(1 - \epsilon\cos(\Omega t))$, i.e. P_0 is the mean ambient pressure. This last equation is a close approximation to the pressure distribution in a liquid subject to a sound field the wavelength of which is large compared with the bubble radius. The nature of the liquid is described by its density ρ_L, surface tension σ, and viscosity μ. It is assumed that the amount of vapor in the bubble is negligible, and that P_{in} can be written in the form $P_{in} = P_{in,eq}(R_0/R)^{3k} - 4\mu_{th}x'$, where k is the polytropic exponent determined in step 1 and $P_{in,eq}$ is the internal pressure corresponding to the equilibrium radius R_0. This is the pressure-volume equation. As in step 1, we are interested in the oscillations of the bubble about R_0. Recall that x(t), the fractional radial deviation, is defined by $R(t) = R_0(1 + x(t))$. In order to use the minimal number of parameters in the differential equation for x it is advisable to express all the variables is terms of a dimensionless time τ (tau) defined by $\tau = (P_{in,eq}/\rho_L)^{\frac{1}{2}}(t/R_0)$. Note that differentiation of x is now with respect to τ (tau), defined below. Such derivatives are denoted with dots over x.

We assume that x and its time derivatives are small enough so that when Taylor expansions for these quantities are substituted into Rayleigh's equation we may neglect terms of 4th and higher order in x and its derivatives (to describe nonlinear behavior it is necessary to retain at least the x^2 terms as well as the x^1 terms; if only the x^1 terms are retained then the expansion becomes a simple linearization). The fact that the values of the parameters 'k' and 'μ' (used below) are estimated using first order expansions of the terms in the mass, energy, and momentum balances means that, strictly speaking, they are valid only for a linear system. Their usage when analyzing this nonlinear system is an *ad hoc* approach necessitated by the complicated nature of the mathematics.

After substituting the resulting Taylor polynomials into Rayleigh's equation we obtain a low-order version of Rayleigh's equation expressed in

terms of x:

$$\ddot{x} + \omega_0^2 x = \delta\cos(\omega\tau) + [-1.5(\dot{x})^2 + \alpha_1 x^2 - \delta x\cos(\omega\tau) - 2b(\dot{x})] + [1.5(\dot{x})^2 x - \alpha_2 x^3 + \delta x^2\cos(\omega\tau) + 4b\, x\, (\dot{x}) \qquad [A2]$$

where $\alpha_1 = 4.5(k(k+1)) - 2W$, $\alpha_2 = 0.5k(9k^2 + 18k + 11) - 3W$,
$W = 2\sigma/(R_0 P_{in,eq})$, $b = 2\mu_{eff}/(R_0(\rho_L P_{in,eq})^{\frac{1}{2}})$, $\delta = (1 - W)\epsilon$
$dimfac = R_0(\rho_L/P_{in,eq})^{\frac{1}{2}}$, $\omega_0^2 = \Omega_0^2(dimfac)^2$, $t/\tau = dimfac$
Note that Ω and Ω_0 are dimensionalized frequencies (e.g., in MHz) whereas 'ω' and 'ω_0' are non-dimensionalized frequencies.

Step 3: Because we will use the bubble detector to measure only the 2ω component of the radiated pressure wave, and since the radiated pressure is proportional to the second derivative of the fractional radial deviation $x(\tau)$, we restricted our calculations to those resonance solutions $x(\tau)$ that have a 2ω component. Careful examination of the complicated expressions for the resonance solutions to equation [A2] shows that only the main resonance and first (ultra)harmonic solutions satisfy this requirement. The 2ω component of the solution that is valid near the first harmonic frequency ($\omega_0/2$) is $x(\tau) = C\cos(2\omega\tau + \phi)$, where the amplitude C has (as expected) three possible values. These values can be determined by solving a cubic polynomial. (This polynomial has very complicated coefficients; see [2], p.880.) The three values of C correspond to the three solutions that are valid only near the first harmonic frequency. Which solution is encountered in a given experiment depends on the initial conditions and whether an upward or downward sweep of driving frequencies is being performed (see discussion of hysteresis above). Because we are interested in calculating only the amplitude of $\ddot{x}(\tau)$, denoted $|\ddot{x}|$, it is not necessary to compute the phase shift ϕ. (If ϕ were needed, one could calculate it.) Clearly $|\ddot{x}(\tau)| = 4C\omega^2$.

The 2ω component of the main resonance solution is more complicated. It turns out to be $x(\tau) = -.25A_1\cos(2\omega\tau - \phi) - .25B_1\cos(2\omega\tau + 2\phi)$ where $A_1 = -2\omega^2 z\delta C$, $B_1 = 2\omega^2 z(\alpha_1 + (1.5)\omega^2) C^2$, and $z = 1/(4\omega^2 - \omega_0^2)$. Finding the

amplitude of $\ddot{x}(\tau)$ requires the use of some simple trigonometric identities. If we define $A_2 = A_1\cos(\phi) + B_1\cos(2\phi)$ and $B_2 = A_1\sin(\phi) - B_1\sin(2\phi)$ then the amplitude of $|\ddot{x}(\tau)| = (A_2^2 + B_2^2)^{\frac{1}{2}}$. Calculating the three pairs of values for C and ϕ involves solving a system of two complicated algebraic equations in C and ϕ (see [2], p. 881). We solve these in our Fortran program using a Newton-Raphson subroutine. Each of the three pairs of values corresponds to a solution that is valid only near the main resonance frequency.

Once the amplitude of the 2ω component of a resonance solution has been calculated it is an easy matter to compute the amplitude of the radiated pressure wave corresponding to it. Letting $|\ddot{x}|$ denote the amplitude of the second derivative of the 2ω-component of a solution x(t), it is not hard to show that the amplitude of the corresponding P_{rad}, denoted $|P_{rad}|$, satisfies

$$|P_{rad}| = (\rho_L R_0^3/r)|\ddot{x}|(1 + (\Omega R_0/c)^2)^{-\frac{1}{2}} \qquad [A3]$$

where r is the distance from the transducer head of the detector to the bubble and c is the speed of sound in the liquid. We convert $|P_{rad}|$ to a voltage amplitude using gain factors that are specific to our bubble detection hardware. By comparing the measured voltage amplitudes near the two resonance frequencies with the predicted values, one can estimate R_0, the equilibrium bubble radius. This involves use of standard statistical parameter estimation procedures; see "Data Handling" section of the main report for details.

References:

A1. E. Atlee Jackson, Perspectives of Nonlinear Dynamics vol. 1, Cambridge University Press, 1989.

A2. D. W. Jordan and P. Smith, Nonlinear Ordinary Differential Equations (2nd ed.), Oxford University Press, 1987.